Postprint of: Lech R., Marynowski W., Kusiek A., An Analysis of Elliptical-Rectangular Multipatch Structure on Dielectric-Coated Confocal and Nonconfocal Elliptic Cylinders, IEEE Transactions on Antennas and Propagation, Vol. 63, Iss. 1 (2015), pp. 97-105, DOI: 10.1109/TAP.2014.2365573

An Analysis of Elliptical-Rectangular Multipatch Structure on Dielectric-Coated Confocal and Non-Confocal Elliptic Cylinders

Rafal Lech, Adam Kusiek, Wojciech Marynowski

***Abstract*—A rigorous analysis of the resonance frequency problem of an elliptical-rectangular microstrip structure mounted on dielectric coated elliptic conducting cylinder, with electrically small radius, is investigated in this paper. A full-wave analysis and a moment-method calculation are employed. The analysis is carried out considering the expansion of the field as a series of Mathieu functions. The complex resonance frequencies of the structure are studied. Modes suitable for antenna application are also investigated. Numerical results for the complex resonance frequency and radiation patterns are calculated and verified by comparing them with results from commercial software and our own measurements of manufactured prototypes. The difference between confocal and non-confocal dielectric coated elliptic cylinders is investigated.**

***Index Terms*—Microstrip antenna arrays, elliptical-rectangular structure, method of moments, complex resonance frequency, antenna radiation patterns, confocal, non-confocal.**

I. Introduction

CONFORMAL microstrip structures find many practical applications in airplanes, spacecraft, speedboats and other high-speed vehicles where aerodynamic or hydrodynamic considerations necessitate their use. The most common application of such structures are in conformal antennas. Due to the possibility of their merging into curved surfaces they can also be utilized on the walls of buildings, towers or columns without disturbance of the aesthetics of the building and local architecture. Another advantage of utilizing conformal antennas arises from electromagnetic considerations and the need to obtain the specific radiation characteristics. Antennas with curved surfaces provide a higher visible range compared to planar antennas. An example of such a structure would be a circular antenna array or an array of radiators located on the surface of a cylinder, which provide omni-directional radiation patterns in the azimuth plane, or else provide, in this plane, the possibility of beam control [1].

The methods of analysis of conformal antenna are commonly divided according to the point of view of antenna dimensions [1]. Electrically small antennas are often analyzed using orthogonalization and mode-matching methods [2] [3], the method of moments combined with integral equations [4]–[10], the finite element method, often combined with other approaches [11], and the finite-difference time-domain method [12]. Large antennas are mainly analyzed with the use of a high-frequency approach, which uses various asymptotic techniques to find approximate solutions, often combined with the method of moments [13]–[15] to take into account small details in the antenna structure geometry.

Antennas printed on layered circular cylinders have been fully investigated and described in the literature. However, a more interesting and more general case is the elliptic-cylindrical body, which allows surfaces to be investigated with variable radius of curvature and model, e.g., wings and tails of airplanes. The analysis of elliptical bodies is mainly considered for the scattering problems [16]–[18]. The case of antennas printed on elliptic-cylindrical surfaces has so far been considered only in a few papers. The results for radiation by sources placed on metallic surfaces based on asymptotic techniques can be found in [19], [20]. A cavity-backed patch antenna mounted on an elliptic cylinder was analyzed in [21]. Axial slot antennas on conducting elliptic cylinders with a dielectric coating were investigated in [22], [23]. The results of resonance frequencies and radiation patterns calculation using cavity model analysis of a rectangular patch antenna printed on a thin elliptic-cylindrical substrate, using the approximation of constant dielectric layer thickness for confocal ellipses, can be found in [24] and [25].

In this paper, a complex resonant frequency problem of an elliptical-rectangular microstrip structure mounted on elliptical cylinder with a dielectric substrate layer is investigated. Both confocal and non-confocal cases of dielectric-coated conducting elliptic cylinder are considered. The thickness of the substrate layer is assumed to be irregular in the case of confocal ellipses and constant in the case of non-confocal ellipses. A full-wave analysis and a moment-method calculation are employed. The analysis is carried out considering the expansion of the field as a series of Mathieu functions. For the analysis of the non-confocal case the additional theorem for Mathieu functions is utilized. The proposed model can be easily extended to take in to account the additional layers in the antenna structure (dielectric antenna covers or air gaps in substrate or superstrate layers) by using procedure presented by authors in [10] for patch antennas configurations on circular cylinder. Also, to the best knowledge of the authors of this article, the comparison between microstrip structures placed on confocal and non-confocal dielectric-coated conducting elliptic

R. Lech, A. Kusiek and W. Marynowski are with the Department of Microwave and Antenna Engineering, Faculty of Electronics, Telecommunications and Informatics, Gdansk University of Technology, Gdansk, 80-233 Poland e-mail: rafal.lech@eti.pg.gda.pl, adakus@eti.pg.gda.pl, wojmar@eti.pg.gda.pl.

This work was supported from sources of National Science Center under grant decision no. DEC-2011/01/D/ST7/06639.

Manuscript received MMMM DD, 2014; revised MMMM DD, 2014.

cylinders is presented for the first time. From this comparison it is evident that the approximation of constant dielectric layer thickness for confocal ellipses case, even for a thin elliptic-cylindrical substrate, is incorrect. The complex resonance frequencies and radiation patterns for the chosen examples are calculated and the results are verified by comparing them with those obtained from a commercial simulator and our own measurements of manufactured prototypes.

II. Formulation of the Problem

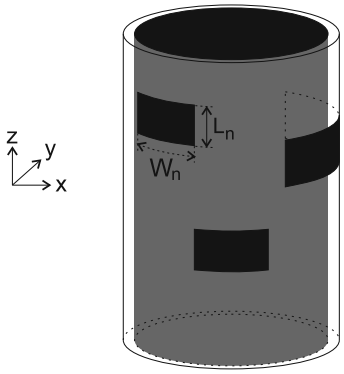

Fig. 1. The geometry of an investigated structure - multipatch microstrip structure on elliptical body.

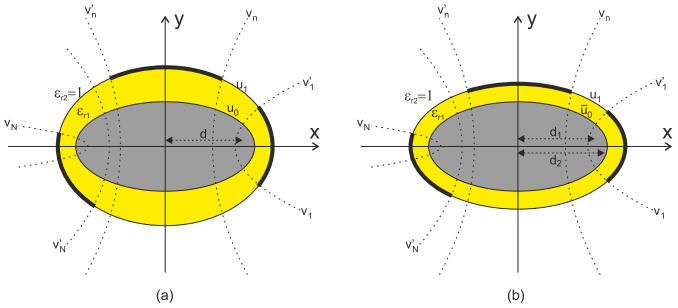

Fig. 2. The cross-section of the structure; (a) confocal ellipses; (b) non-confocal ellipses.

The investigated structure is composed of N ($n = 1, \ldots, N$) patches located on an elliptical surface with an elliptical cylinder axis along the $\vec{i}_z$ direction, as schematically illustrated in Fig. 1. Two versions of the microstrip structure are investigated: in the first one the conducting cylinder and the dielectric layer are built from confocal ellipses (see Fig. 2(a)), while in the second they are built from non-confocal ellipses (see Fig. 2(b)). Here u and v are the radial and the angular coordinates, respectively, and d is the focal length. The patches are placed on a substrate layer with relative permittivity ε_{r1}. Each patch is of length L_n (along the z axis) and width W_n (along the v axis), and is located arbitrarily on the elliptical surface, i.e., between v_n and v'_n along the v axis and between z_n and z'_n along the z axis on the surface with u_1. The contour of the conducting cylinder is placed in $u = u_0$, and the interface between dielectric layer and air space is placed in $u = u_1$. In the case of confocal ellipses both u_0 and u_1 interfaces are defined in the same elliptical coordinate system with focal length d. In the case of non-focal ellipses the ellipses have different focal length (d_1 for the ellipse of conducting cylinder and d_2 for the interface between dielectric layer and air space), and therefore the interfaces are denoted as $\bar{u}_0$ and u_1 (a line above the variable will indicate the coordinate system for the inner ellipse while the variable without the line will denote the coordinate system of the outer ellipse).

In the analysis of the confocal ellipses case, the contour of the conducting cylinder and the dielectric layer have the same focal length, which simplifies the analysis of the structure. For the non-confocal ellipses case, both contours have different focal lengths and the analysis of such structure requires the use of an additional theorem for the Mathieu functions [26], which increases the complexity of analysis. In the case when the values of both minor and major axes of the ellipses are equal, which indicates that the structure has circular cross-sections, both confocal and non-confocal cases are identical. However, with the decreasing minor-over-major axis ratio the thickness of the dielectric layer, in the case of confocal ellipses, becomes irregular. The more elliptical structure (lower value of minor-over-major axis) the higher irregularity of the dielectric layer thickness and in result the bigger difference between the height of the dielectric layer under the patch edges and its center (see Fig. 2(a)). Furthermore the irregular thickness of the dielectric layer is somewhat difficult to realize in practical application. In the literature it is sometimes assumed that for thin dielectric layers ($u_1 - u_0 \ll u_0$), and assuming that $(d\cosh(u_1) - d\cosh(u_0)) \ll \lambda$ the substrate thickness can be considered as constant at any value of the angular coordinate. However, as will be shown in the results section, this assumption, even for thin layers, does not always lead to correct results.

It is assumed that the patches are made of an ideal conductor, and therefore that on the patch surfaces the tangential components of the electric field are zero. Utilizing this condition the unknown surface currents on the patches can be found. The structure is divided into two regions: a dielectric layer and an air space outside the structure. The z components of the electric and magnetic fields, due to the current distribution on the patch in each region, have the following form (suppressing $e^{-i\omega t}$ time dependence):

$$F_z^{(\kappa)}(u,v,z) = \frac{1}{2\pi}\int_{-\infty}^{\infty} dk_z e^{ik_z z} \times \sum_{\nu}\left(\sum_{l=0}^{L} M_{cl}^{(\nu)}(u,q_\kappa)A_{l,\kappa}^{(\nu),\zeta,e} ce_l(v,q_\kappa) + \sum_{l=1}^{L} M_{sl}^{(\nu)}(u,q_\kappa)A_{l,\kappa}^{(\nu),\zeta,o} se_l(v,q_\kappa)\right) \quad (1)$$

where $F,\zeta = \{E,H\}$ relate the functions and coefficients to electric or magnetic fields. $\kappa = \{1,2\}$ denote the region. $M_{cl}^{(\nu)}(\cdot)$ and $M_{sl}^{(\nu)}(\cdot)$ are even and odd radial Mathieu functions, respectively, of order l and kind $\nu = \{1,4\}$. $ce_l(\cdot)$ and $se_l(\cdot)$ are even and odd angular Mathieu functions, respectively, of order l. $A_{l,\kappa}^{(\nu),\zeta,e(o)}$ are unknown coefficients relevant

to even (e) and odd (o) functions of order l and kind ν and they will be determined by satisfying the boundary conditions. The parameters q_κ are related to the transverse propagation constant k_z as $q_\kappa = (k_\kappa^2 - k_z^2)d^2/4$, where $k_\kappa = \omega\sqrt{\varepsilon_{r\kappa}\varepsilon_0\mu_0}$. In the case of non-confocal ellipses, in the dielectric layer, this parameter will be defined for focal length d_1 as $\bar{q}_1$ and for focal length d_2 as q_1.

The v components of the electric and magnetic fields can easily be obtained from z components:

$$E_v = \frac{1}{h(k_\kappa^2 - k_z^2)}\left(\frac{\partial^2 E_z}{\partial z \partial v} + i\omega\mu\frac{\partial H_z}{\partial u}\right) \tag{2}$$

$$H_v = \frac{1}{h(k_\kappa^2 - k_z^2)}\left(\frac{\partial^2 H_z}{\partial z \partial v} - i\omega\varepsilon\frac{\partial E_z}{\partial u}\right) \tag{3}$$

where $h = d\sqrt{\cosh^2(u) - \cos^2(v)}$.

In the outer region the coefficients $A_{l,2}^{(1),\zeta,e(o)} = 0$, and in region 1, applying the boundary condition on the tangential components of the electric field (E_z and E_v) at $u = \bar{u}_0$ the coefficients $A_{l,1}^{(4),\zeta,e(o)}$ take the following form:

$$A_{l,1}^{(4),E,e(o)} = -\frac{M_{c(s)l}^{(1)}(\bar{u}_0, \bar{q}_1)}{M_{c(s)l}^{(4)}(\bar{u}_0, \bar{q}_1)} A_{l,1}^{(1),E,e(o)}, \tag{4}$$

$$A_{l,1}^{(4),H,e(o)} = -\frac{M_{c(s)l}^{'(1)}(\bar{u}_0, \bar{q}_1)}{M_{c(s)l}^{'(4)}(\bar{u}_0, \bar{q}_1)} A_{l,1}^{(1),H,e(o)} \tag{5}$$

where prime indicates derivatives of radial Mathieu functions with respect to the u variable. For the considered structure we obtain eight sets of unknown coefficients (each set of even coefficients is composed of $L+1$ elements, and each set of odd coefficients has L elements).

In order to calculate the resonance frequencies and radiation patterns of the structure the unknown coefficients of the fields in the structure need to be derived. Following the procedure in [10] we write the boundary conditions for the tangential components of the electric and magnetic fields in the spectral domain at the interface $u = u_1$ and rearrange them to take the following form:

$$\begin{aligned}
&\tilde{H}_z^{(2)}(v, u_1, k_z) - \tilde{H}_z^{(1)}(v, u_1, k_z) = -\tilde{J}_v(v, k_z)\\
&\tilde{H}_v^{(2)}(v, u_1, k_z) - \tilde{H}_v^{(1)}(v, u_1, k_z) = \tilde{J}_z(v, k_z)\\
&\tilde{E}_z^{(2)}(v, u_1, k_z) - \tilde{E}_z^{(1)}(v, u_1, k_z) = 0\\
&\tilde{E}_v^{(2)}(v, u_1, k_z) - \tilde{E}_v^{(1)}(v, u_1, k_z) = 0
\end{aligned} \tag{6}$$

where $\tilde{J}_v(v, k_z)$ and $\tilde{J}_z(v, k_z)$ are patch surface current densities in the spectral domain defined as follows:

$$\begin{bmatrix}\tilde{J}_v(v, k_z)\\ \tilde{J}_z(z, k_z)\end{bmatrix} = \frac{1}{2\pi}\int_{-\infty}^{\infty} dz e^{-ik_z z}\begin{bmatrix}J_v(v, z)\\ J_z(v, z)\end{bmatrix} \tag{7}$$

In order to solve the boundary problem (6) for the non-confocal ellipses, the fields in the dielectric layer (region 1) need to be transformed from the elliptical coordinate system of the conducting cylinder to an elliptical coordinate system of the interface between dielectric layer and air space. The transformation is applied using the additional theorem of Mathieu functions, as described in appendix A. Applying Galerkin's method to (6), and using angular Mathieu functions from outer region $ce_l(v, q_2)$ and $se_l(v, q_2)$ as testing functions, we obtain eight equations. These equations are then rearranged and rewritten in matrix form as follows:

$$\begin{bmatrix}\mathbf{X}_{11} & \mathbf{X}_{12}\\ \mathbf{X}_{21} & \mathbf{X}_{22}\end{bmatrix}\begin{bmatrix}\mathbf{A}_c\\ \mathbf{A}_r\end{bmatrix} = \begin{bmatrix}\tilde{\mathbf{J}}\\ \mathbf{0}\end{bmatrix} \tag{8}$$

where vector $\mathbf{A}_c$ contains four sets of amplitudes from the chosen region. In the case of calculating the radiation patterns the best choice is to pick the amplitudes of the fields in the outer region. When the resonance frequencies of the antenna are calculated it is suitable to pick the amplitudes of the fields in regions located above or below the patch. Therefore, for the investigated structure, vector $\mathbf{A}_c$ contains the amplitudes from the outer region and has the following form:

$$\mathbf{A}_c = \left[\mathbf{A}_2^{(4),E,e}, \mathbf{A}_2^{(4),E,o}, \mathbf{A}_2^{(4),H,e}, \mathbf{A}_2^{(4),H,o}\right]^T \tag{9}$$

where $\mathbf{A}_2^{(4),(\cdot),o} = [A_{1,2}^{(4),(\cdot),o}, \ldots, A_{L,2}^{(4),(\cdot),o}]$, and $\mathbf{A}_2^{(4),(\cdot),e} = [A_{0,2}^{(4),(\cdot),e}, A_{1,2}^{(4),(\cdot),e}, \ldots, A_{L,2}^{(4),(\cdot),e}]$. Vector $\mathbf{A}_r$ contains all the other amplitudes. The current densities vector is arranged as:

$$\tilde{\mathbf{J}}(k_z) = [\tilde{\mathbf{J}}_v^e(k_z), \tilde{\mathbf{J}}_v^o(k_z), \tilde{\mathbf{J}}_z^e(k_z), \tilde{\mathbf{J}}_z^o(k_z)]^T \tag{10}$$

where the elements of vectors $\tilde{\mathbf{J}}_{v(z)}^{e(o)}(k_z)$ have the following form:

$$\left(\tilde{\mathbf{J}}_{v(z)}^e(k_z)\right)_{l=0}^{L} = \int_0^{2\pi} dv \;\; ce_l(v, q_2)\tilde{J}_{v(z)}(v, k_z), \tag{11}$$

$$\left(\tilde{\mathbf{J}}_{v(z)}^o(k_z)\right)_{l=1}^{L} = \int_0^{2\pi} dv \;\; se_l(v, q_2)\tilde{J}_{v(z)}(v, k_z) \tag{12}$$

Matrices $\mathbf{X}_{11}$, $\mathbf{X}_{12}$, $\mathbf{X}_{21}$ and $\mathbf{X}_{22}$ are square matrices of size $2(2L+1)$. The elements of these matrices are given in appendix A.

From (8), the relation between chosen coefficients and patch surface current densities can be derived:

$$\mathbf{A}_c = \left(\mathbf{X}_{11} - \mathbf{X}_{12}\mathbf{X}_{22}^{-1}\mathbf{X}_{21}\right)^{-1}\tilde{\mathbf{J}} = \mathbf{X}'\tilde{\mathbf{J}} \tag{13}$$

Obtaining the unknown coefficients $\mathbf{A}_c$, the expressions for the transverse electric fields of E_z and E_v on all patch surfaces in the outer region can be written as follows [9]:

$$\begin{aligned}\mathbf{E}(u_1, v, z) \;\; &= \;\; \frac{1}{2\pi}\int_{-\infty}^{\infty} dk_z e^{ik_z z}\\ &\times\mathbf{Y}(u_1, v, k_z)\mathbf{X}'(k_z)\tilde{\mathbf{J}}(k_z) = 0\end{aligned} \tag{14}$$

where the electric vector $\mathbf{E} = (E_v(\cdot), E_z(\cdot))^T$ and the elements of matrix $\mathbf{Y}$ are as defined in appendix B.

The integral equation (14) is solved using Galerkin's moment method. Following Galerkin's procedure, the surface current densities on the nth patch are expanded in terms of a linear combination of known basis functions:

$$\vec{J}(v, z) = \sum_{m_1=1}^{M_{1,n}} I_{v,m_1}^{(n)} J_{v,m_1}^{(n)}(v, z)\vec{i}_v + \sum_{m_2=1}^{M_{2,n}} I_{z,m_2}^{(n)} J_{z,m_2}^{(n)}(v, z)\vec{i}_z \tag{15}$$

where $I_m^{(n)}$ denotes unknown coefficients for the mth basis function for the nth patch. The most common choices of basis functions are those obtained from the cavity-model functions [24], [27], which take the following form:

$$J_{vm_1}^{(n)}(v,z) = \sin\frac{m_{1v}\pi s_n}{S_n}\cos\frac{m_{1z}\pi(z-z_n)}{z_n'-z_n} \quad (16)$$

$$J_{zm_2}^{(n)}(v,z) = \cos\frac{m_{2v}\pi s_n}{S_n}\sin\frac{m_{2z}\pi(z-z_\xi)}{z_\xi'-z_\xi} \quad (17)$$

where $m_v, m_z = 0, 1, \ldots, \infty$ and their combination denotes the mode number of the basis function. S_n is the length of elliptical arc covered by the current distribution, which is equal to the width W_n of the nth patch, and s is the curvilinear coordinate that follows the arc.

The spectral amplitudes of the current distribution are calculated from:

$$\tilde{J}(v,k_z) = \frac{1}{2\pi}\int_{z_n}^{z_n'} dz e^{-ik_z z} J(v,z) \quad (18)$$

Substituting the calculated spectral components of the current distributions into (14) and then using the chosen basis functions as testing functions and integrating the obtained equation over the patch area, the following matrix equation is obtained:

$$\begin{bmatrix}\mathbf{Z}_{vv} & \mathbf{Z}_{vz}\\ \mathbf{Z}_{zv} & \mathbf{Z}_{zz}\end{bmatrix}\begin{bmatrix}\mathbf{I_v}\\ \mathbf{I_z}\end{bmatrix} = 0 \quad (19)$$

In the results section the resonance frequencies of single-patch configurations are shown, whereby $\mathbf{I_{v(z)}}$ in (19) has the following form:

$$\mathbf{I_{v(z)}} = [I_{v(z),1}, \ldots, I_{v(z),M_{1(2)}}]^T \quad (20)$$

where $M_{1(2)}$ is the number of modes for the patch antenna.

The terms of the sub-matrices $\mathbf{Z}_{(\cdot)}$ are defined as follows:

$$[\mathbf{Z}_{x,y}]_{pr} = \int_{-\infty}^{\infty} dk_z \int_{v_n}^{v_n'} dv \; \tilde{\mathbf{J}}_{x,p}(v,-k_z)\mathbf{Y}(u_1,v,k_z)\mathbf{X}'(k_z)\tilde{\mathbf{J}}_{y,r}(k_z) \quad (21)$$

where $x, y = (v, z)$, p and r denote the mode number for the structure.

Non-trivial solutions can exist if the determinant of (19) vanishes, that is, $\det(\mathbf{Z}) = 0$. This is the eigenvalue equation, the roots of which are complex frequencies $f = \mathfrak{Re}f + j\mathfrak{Im}f$ for a particular mode [7]. This complex frequency gives the resonant frequency $\mathfrak{Re}f$ and the quality factor $\mathfrak{Re}f/2\mathfrak{Im}f$ for the microstrip patch. The imaginary part of the complex resonance frequencies accounts for the radiation losses [8].

The far-zone radiated fields in the spherical coordinates are given by [9]:

$$\begin{bmatrix}E_\theta\\ E_\phi\end{bmatrix} \cong \frac{1}{\sin\theta}\begin{bmatrix}-1 & 0\\ 0 & \sqrt{\frac{\mu_0}{\varepsilon_0}}\end{bmatrix}\begin{bmatrix}E_z\\ H_z\end{bmatrix} \quad (22)$$

In the far field ($r \to \infty$) the z components of electric and magnetic fields have the following form:

$$F_z = \frac{-ie^{ik_0 r}}{\pi r}\left[\sum_{l=0}^{L}(i)^l ce_l(v,q_2)A_2^{(4),F,e}(k_0\cos\theta) + \sum_{l=1}^{L}(i)^l se_l(v,q_2)A_2^{(4),F,o}(k_0\cos\theta)\right] \quad (23)$$

where $F = \{E, H\}$. To calculate the radiation pattern the field coefficients need to be calculated from (13), assuming $k_z = k_0\cos\theta$, and introduced into (23).

III. Results

In this section the numerical results of several chosen configurations are presented. The calculations of the resonant frequencies of TM_{10} mode (the patch current is excited in the v direction) and TM_{01} mode (the patch current is excited in the z direction) of single-patch configurations placed on different sides of the ellipse versus the minor-over-major axis ratio a_{min}/a_{max} of the cylinder are performed. The comparison between the confocal and non-confocal cases is made and the obtained results are compared with the calculations of the commercial software simulator ANSYS HFSS. The radiation patterns for the chosen single patches and patches arrays are established and the obtained results are also compared with the HFSS calculations, as well as our own measurements.

Similarly to the case of the microstrip structure on the circular cylinder along the original path of integration, branch-point singularities and pole singularities are encountered [28] [29], which makes the integrals (21) non-integrable along the real axis on the complex k_z plane. To avoid these branch-point singularities, the deformed path proposed in [29] and applied in [10] is utilized here (see Fig. 3), where $P1 = k_0(1 - iT_1)$, $P2 = k_0\sqrt{1+T_2^2}$, $P3 = k_0\sqrt{1+T_3^2}$. For the presented examples, to obtain accurate results, the values of these parameters are as follows: $T_1 \in [0.2, 0.5]$, $T_2 \in [20, 30]$, and $T_3/T_2 \in [1.1, 5]$. Also for the presented examples, to calculate resonance frequencies, it was sufficient to select $L = 30$ terms for the convergence of the l-series of (1), (11) and (12). For radiation pattern calculation, $L = 10$ terms were found to be sufficient for the convergence of these series.

It should be noticed that the truncation of the l-series is dependent on the radius and/or frequency of the host elliptical cylinder. The larger value of the cylinder radius (in electrical sense), the larger number of l-series truncation should be taken to obtain convergent results. Unfortunately, utilizing a large number of cylindrical special functions with complex arguments and high orders leads to numerical instabilities in the Hankel functions (which are used to calculate Mathieu functions) during the computation of the related spectral Green's functions. Therefore, the presented technique is valid only for elliptical cylinders with electrically small-radius.

In order to calculate the resonance frequency in ANSYS HFSS for a specific mode (TM_{10} or TM_{01}) the patch needed to be fed by a coaxial line. To excite the TM_{10} mode the feeding point needs to be displaced from the patch center along its width (along v coordinate), while to excite TM_{01} mode the

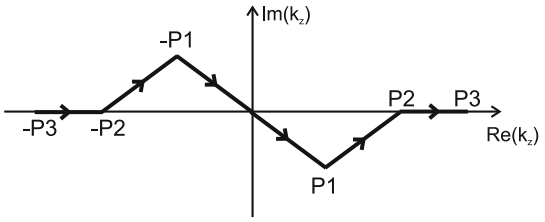

Fig. 3. Deformed integration path.

feeding point needs to be displaced from the patch center along its height (along z coordinate).

The calculations of the proposed model were performed in MATLAB environment on Intel Xenon X5690 3.47 GHz (2 processors). Assuming $L = 30$ terms in the series, the calculation of a single frequency point takes approximately 15 seconds. Comparing this to the calculation of commercial software ANSYS HFSS the time of single frequency point calculation is 81 seconds with 516 seconds of adaptive process. The difference between the effectiveness of our method with respect to HFSS is not surprising, since the developed model is dedicated only to the structures considered in the article. However, the results clearly shows that such model is suitable and more predisposed to utilize in the optimization process.

A. Resonant frequencies

As an example, the structure investigated in [24] is chosen. The patch of width $W = 4$ cm and length $L = 3$ cm (see Fig. 1) is printed on the ellipse with major axis $a_{max} = 5$ cm, and is coated with a dielectric with $\varepsilon_r = 2.32$ and thickness $h = 0.795$ mm. Two patch positions are considered, which will be denoted as type I and type II. In the type-I structure the center of the patch is located along the x axis (see Fig. 4(a)), and in the type-II structure along the y axis (see Fig. 4(b)). To obtain different ratios a_{min}/a_{max}, spanning from 0.3 to 0.999, the y-directed minor axis of the ellipse is changed. Both confocal with irregular dielectric thickness and non-confocal with constant dielectric thickness cases are considered.

Figs. 5 and 6 show the complex resonance frequencies of the TM_{10} and TM_{01} mode, respectively, for the structure types I and II as functions of the ratio a_{min}/a_{max} of the cylinders.

To find the complex roots of the characteristic equation a hybrid complex root-finding algorithm [30], which uses an adaptive mesh, based on Delaunay triangulation, to sample the function, was utilized.

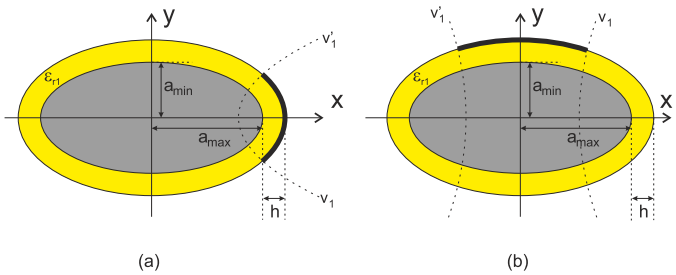

Fig. 4. Single-patch antenna on elliptical body: a) type I - antenna center along x axis; b) type II - antenna center along y axis.

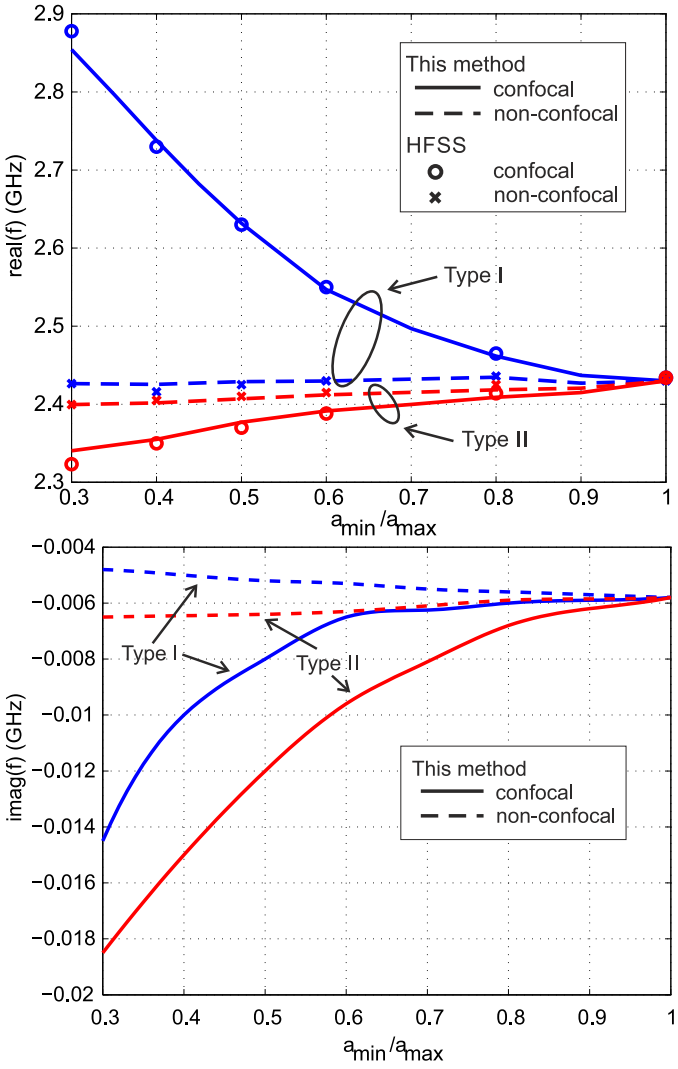

Fig. 5. Real and imaginary parts of resonance frequencies of TM_{10} mode as functions of minor/major axis (a_{min}/a_{max}) of single-patch structure of type I and type II.

As can be observed for both modes, the resonance frequencies of the non-confocal cases with constant dielectric-layer thickness are almost unchanged. However, when the dielectric-layer thickness is irregular (confocal case) the patch resonant frequency changes for both type-I and type-II antenna configurations. The largest changes are visible in the case of the type-I structure for TM_{10} mode, where the resonant frequency shifts by about 400 MHz. It can also be seen that the TM_{01} mode is less sensitive to changes in the patch curvature than the TM_{10} mode. In each case the obtained results are compared with the calculations of HFSS full-wave simulator, and good agreement was observed. The discrepancies between the results, especially for lower values of a_{min}/a_{max} ratio, may be the result of using feeding line in HFSS calculations, however, the error is smaller than 1.2%, which is satisfactory.

In the confocal case for type-II structure, by making the structure more elliptical substrate thickness is increased under the patch surface. The increase in substrate thickness decreases the structure resonance frequency, which is associated with the increase of the effective length of the patch related to the

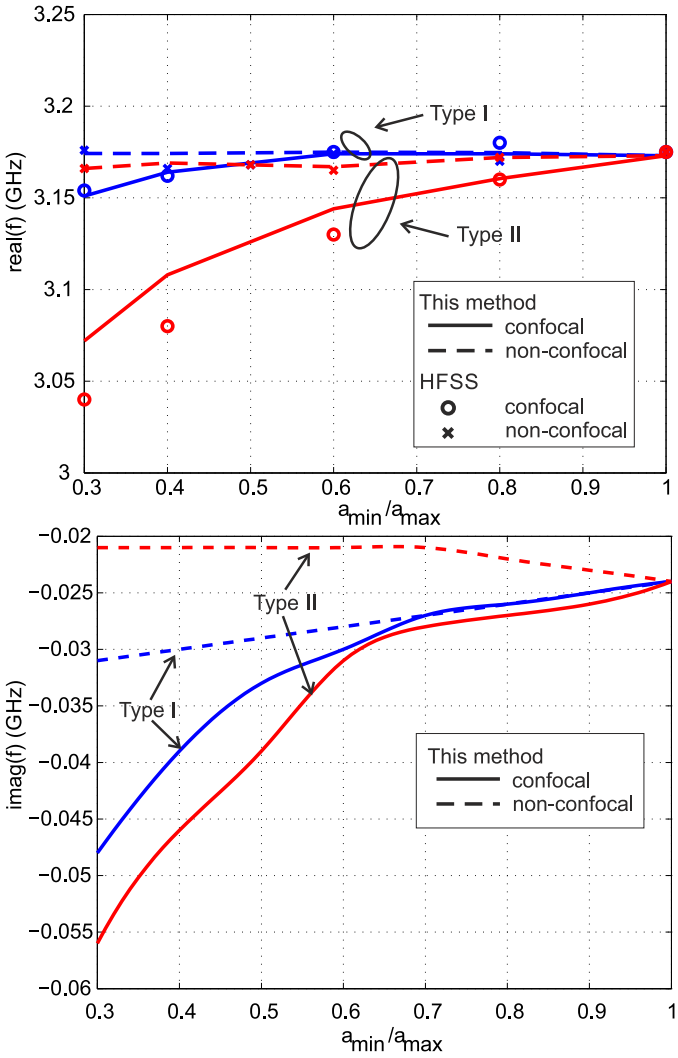

Fig. 6. Real and imaginary parts of resonance frequencies of TM_{01} mode as functions of minor/major axis (a_{min}/a_{max}) of single patch structure of type I and type II

fringing effect on the patch edges. This effect is observed for type-II structure in both modes, as in both these cases the effective length or effective width is increased.

This phenomenon is also observed in planar patch antennas, where by increasing the substrate thickness the capacitance under the patch decreases but at the same time the capacitances on the patch edges (associated with fringing effect of the field) increase, which results in an increase of the overall patch capacitance and therefore a decrease of resonance frequency.

Making the structure more elliptical for type-I structure causes a stronger increase of the substrate thickness at the sides of the patch than at its center (with respect to angular coordinate). The structure behaves differently for each mode. In the case of the TM_{01} mode, mainly the patch length (not width) determines resonance frequency, and the substrate thickness is only increased in the corners of both the upper and lower side of the patch (with respect to the z axis). In this case, for more elliptical structures the resonance frequency behaves similarly to the type-II structure.

In the case of the TM_{10} mode the width of the patch

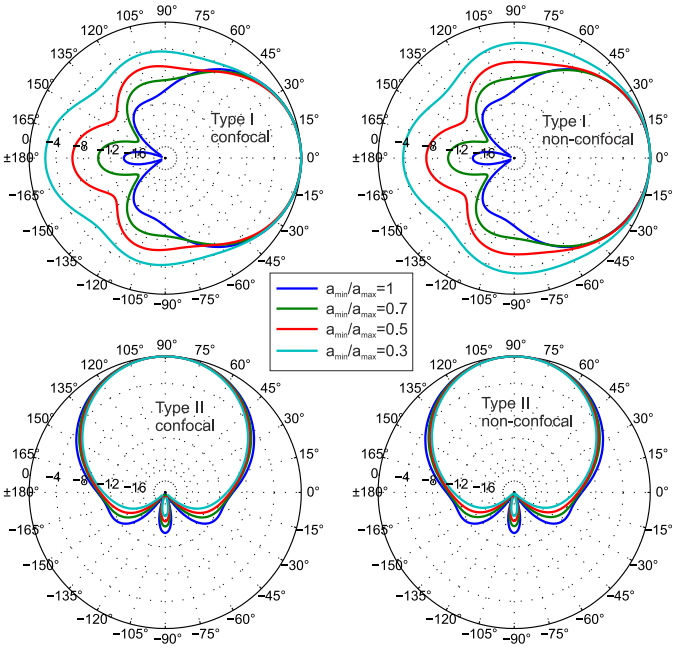

Fig. 7. Normalized radiation patterns around the resonance of TM_{10} mode for rectangular patches of type-I and type-II structures, confocal and non-confocal cases.

has a greater influence on the resonance frequency, and for more elliptical structures the distance between patch edges and the ground (conducting ellipse) is greater than the distance between its center and the ground. For this deformation the fringing effect is weaker in this structure and the overall capacitance under the patch decreases, which in turn increases the resonance frequency.

Comparing the imaginary parts of the complex frequency for confocal and non-confocal cases it is seen that, similar to real parts, the structure with irregular dielectric layer is more affected by the change of its ellipticity than the structure with the layer of constant thickness.

From the performed investigations it is evident that the assumption of constant thickness of the dielectric layer for the confocal case is incorrect, even for thin dielectric layers.

B. Radiation patterns

The radiation patterns of the single-patch configurations for both structure types and both confocal and non-confocal cases were calculated for different ratio a_{min}/a_{max}. The normalized radiation patterns for TM_{10} and TM_{01} modes are illustrated in Figs. 7 and 8, respectively. As can be observed, the patterns of type-II structures are almost unchanged with the variation of ratio e. The biggest change is observed for the TM_{10} mode of type-I structures. The radiation patterns for the confocal and non-confocal cases are almost indistinguishable for the investigated example.

Next, the arrays of three and four rectangular patches located on the circumference of the circular cylinder and elliptical cylinder are investigated. Only the TM_{01} mode and non-confocal case is considered, as only here are the resonant frequencies of the patches the same. Fig. 9 presents the normalized radiation patterns of the investigated configurations

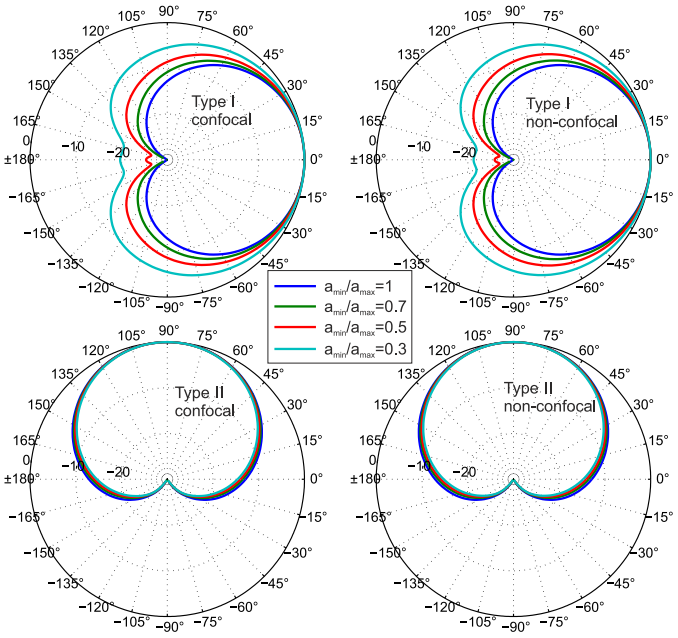

Fig. 8. Normalized radiation patterns around the resonance of TM_{01} mode for rectangular patches of type-I and type-II structures, confocal and non-confocal cases.

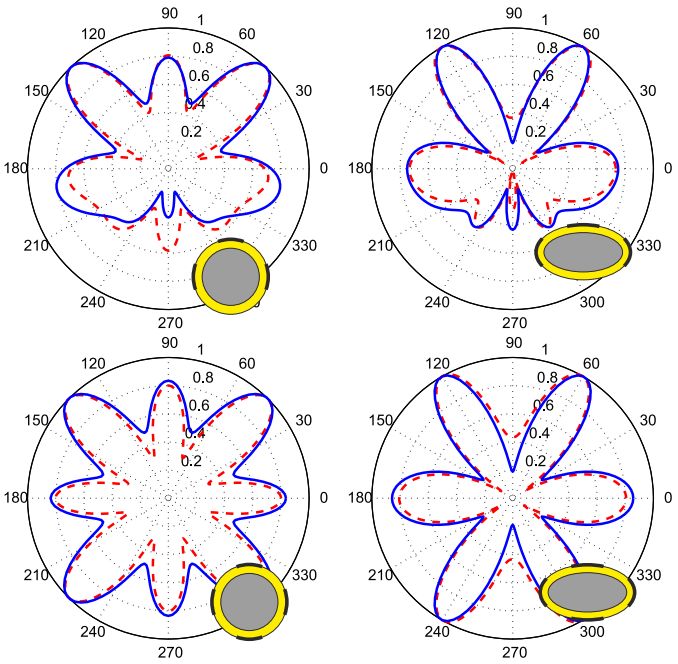

Fig. 9. Normalized radiation patterns around the resonance $f = 1.95$ GHz of TM_{01} mode for the configurations of three and four rectangular patches 4×5 cm on circular cylinder of radius $r = 11.6$cm and elliptical cylinder with major axis $a_{max} = 15$ cm, $a_{min} = 0.5a_{max}$ (non-confocal cases) with dielectric layer of thickness $h = 1$ mm and $\varepsilon_r = 3.44$. Solid line - this method, dashed line - HFSS.

with their cross-sections. In each case the results are compared with those obtained from the Ansoft HFSS simulator, showing satisfactory agreement. The discrepancies may result from the fact that the structures analyzed in HFSS have finite dimensions (along the z axis).

Finally, to additionally check the validity of the proposed

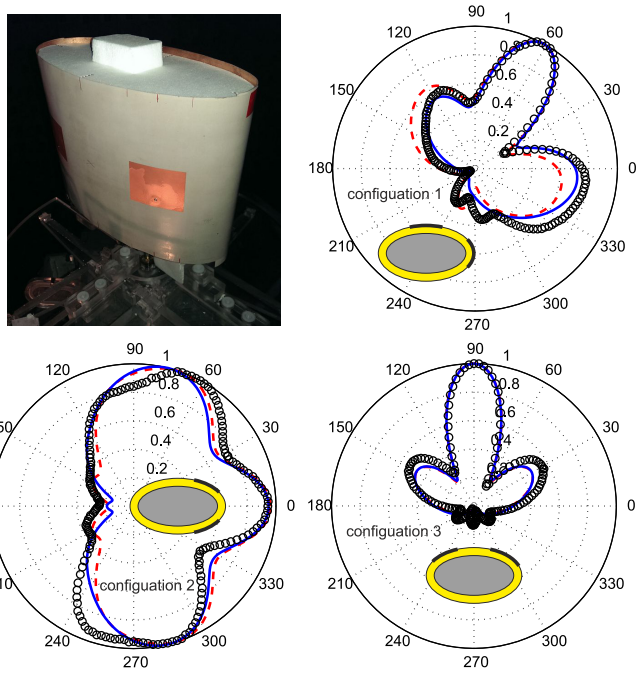

Fig. 10. Normalized radiation patterns around the resonance $f = 1.95$ GHz of TM_{01} mode for three configurations of two rectangular patches 4×5 cm on elliptical cylinder with major axis $a_{max} = 12$ cm $a_{min} = 0.5a_{max}$ with dielectric layer of thickness $h = 0.254$ mm and $\varepsilon_r = 3.44$. The centers of the patches are located in configuration 1 at $v = 0°$ and $90°$, in configuration 2 at $v = -53°$ and $53°$, and in configuration 3 at $v = 53°$ and $127°$. Solid line - this method, dashed line - HFSS, circle line - measurement.

procedure, a double-patch configuration was manufactured and measured, and the obtained results were compared with the calculated ones. The Taconic RF-35 substrate was used with thickness $h = 0.254$ mm and $\varepsilon_r = 3.44$. The manufactured configuration along with obtained results for different patch locations on the elliptical cylinder are presented in Fig. 10. As can be seen, satisfactory agreement between the results was obtained. The discrepancies may have resulted from the manufacturing process of antennas, the feeding system or measurement station in an anechoic chamber.

IV. Conclusion

The procedure for calculating the resonance frequencies and radiation patterns of elliptical-rectangular microstrip structure placed on the surface of a dielectric-coated elliptic conducting cylinder was proposed. A full-wave analysis and a moment-method calculation were employed and the expansion of the field as a series of Mathieu functions was considered. The difference between confocal and non-confocal dielectric-coated elliptic cylinders was investigated. The results showed that the resonance frequency is more affected by the change of structure ellipticity for the case when the dielectric layer is irregular (confocal ellipses) and it changes only slightly when this layer has constant thickness. It was shown that even for thin dielectric layers the assumption of constant thickness for the confocal case does not lead to accurate results. The obtained results were verified by comparing them with calculations of commercial software and our own measurements of manufactured prototype, and good agreement was achieved.

APPENDIX A
THE ELEMENTS OF MATRIX $\mathbf{X}$

Each one of four sub-matrices of matrix $\mathbf{X}$ defined in (8) is a square matrix of size $2(2L+1)$, taking the following form:

$$\mathbf{X}_{11}=\begin{bmatrix} \mathbf{0} & \mathbf{0} & \mathbf{I}^{e_2e_2}\mathbf{H}_2^e & \mathbf{0} \\ \mathbf{0} & \mathbf{0} & \mathbf{0} & \mathbf{I}^{o_2o_2}\mathbf{H}_2^o \\ \mathbf{I}^{e_2e_2}\alpha_2\mathbf{H}_2^{'e} & \mathbf{0} & \mathbf{0} & \mathbf{I}^{e_2o_2'}\vartheta_2\mathbf{H}_2^o \\ \mathbf{0} & \mathbf{I}^{o_2o_2}\alpha_2\mathbf{H}_2^{'o} & \mathbf{I}^{o_2e_2'}\vartheta_2\mathbf{H}_2^e & \mathbf{0} \end{bmatrix}$$

$$\mathbf{X}_{12}=\begin{bmatrix} \mathbf{0} & \mathbf{0} & -\mathbf{I}^{e_2e_1}\mathbf{\Lambda}_H^e & \mathbf{0} \\ \mathbf{0} & \mathbf{0} & \mathbf{0} & -\mathbf{I}^{o_2o_1}\mathbf{\Lambda}_H^o \\ -\mathbf{I}^{e_2e_1}\alpha_1\mathbf{\Lambda}_E^{'e} & \mathbf{0} & \mathbf{0} & -\mathbf{I}^{e_2o_1'}\vartheta_1\mathbf{\Lambda}_H^o \\ \mathbf{0} & -\mathbf{I}^{o_2o_1}\alpha_1\mathbf{\Lambda}_E^{'o} & -\mathbf{I}^{o_2e_1'}\vartheta_1\mathbf{\Lambda}_H^e & \mathbf{0} \end{bmatrix}$$

$$\mathbf{X}_{21}=\begin{bmatrix} \mathbf{I}^{e_2e_2}\mathbf{H}_2^e & \mathbf{0} & \mathbf{0} & \mathbf{0} \\ \mathbf{0} & \mathbf{I}^{o_2o_2}\mathbf{H}_2^o & \mathbf{0} & \mathbf{0} \\ \mathbf{0} & \mathbf{I}^{e_2o_2'}\vartheta_2\mathbf{H}_2^o & \mathbf{I}^{e_2e_2}\beta_2\mathbf{H}_2^{'e} & \mathbf{0} \\ \mathbf{I}^{o_2e_2'}\vartheta_2\mathbf{H}_2^e & \mathbf{0} & \mathbf{0} & \mathbf{I}^{o_2o_2}\beta_2\mathbf{H}_2^{'o} \end{bmatrix}$$

$$\mathbf{X}_{22}=\begin{bmatrix} -\mathbf{I}^{e_2e_1}\mathbf{\Lambda}_E^e & \mathbf{0} & \mathbf{0} & \mathbf{0} \\ \mathbf{0} & -\mathbf{I}^{o_2o_1}\mathbf{\Lambda}_E^o & \mathbf{0} & \mathbf{0} \\ \mathbf{0} & -\mathbf{I}^{e_2o_1'}\vartheta_1\mathbf{\Lambda}_E^o & -\mathbf{I}^{e_2e_1}\beta_1\mathbf{\Lambda}_H^{'e} & \mathbf{0} \\ -\mathbf{I}^{o_2e_1'}\vartheta_1\mathbf{\Lambda}_E^o & \mathbf{0} & \mathbf{0} & -\mathbf{I}^{o_2o_1}\beta_1\mathbf{\Lambda}_H^{'o} \end{bmatrix}$$

where $\alpha_\kappa = -i\omega\varepsilon_0\varepsilon_{r\kappa}/(k_\kappa^2-k_z^2)$, $\beta_\kappa = i\omega\mu_0/(k_\kappa^2-k_z^2)$, and $\vartheta_\kappa = ik_z/(k_\kappa^2-k_z^2)$ for $\kappa=(1,2)$.

$$\begin{aligned} \mathbf{\Lambda}_E^{e(o)} &= \mathbf{J}_1^{e(o)}\mathbf{W}_{e(o)} - \mathbf{H}_1^{e(o)}\mathbf{W}_{e(o)}\mathbf{\Xi}_{e(o)}, \\ \mathbf{\Lambda}_E^{'e(o)} &= \mathbf{J}_1^{'e(o)}\mathbf{W}_{e(o)} - \mathbf{H}_1^{'e(o)}\mathbf{W}_{e(o)}\mathbf{\Xi}_{e(o)}, \\ \mathbf{\Lambda}_H^{e(o)} &= \mathbf{J}_1^{e(o)}\mathbf{W}_{e(o)} - \mathbf{H}_1^{e(o)}\mathbf{W}_{e(o)}\mathbf{\Xi}'_{e(o)}, \\ \mathbf{\Lambda}_H^{'e(o)} &= \mathbf{J}_1^{'e(o)}\mathbf{W}_{e(o)} - \mathbf{H}_1^{'e(o)}\mathbf{W}_{e(o)}\mathbf{\Xi}'_{e(o)}, \end{aligned}$$

with

$$\mathbf{\Xi}_{e(o)} = diag\left(M_{c(s)l}^{(1)}(\bar{u}_0,\bar{q}_1)/M_{c(s)l}^{(4)}(\bar{u}_0,\bar{q}_1)\right)_{l=0(1)}^{L}$$

$$\mathbf{\Xi}_{'e(o)} = diag\left(M_{c(s)l}^{'(1)}(\bar{u}_0,\bar{q}_1)/M_{c(s)l}^{'(4)}(\bar{u}_0,\bar{q}_1)\right)_{l=0(1)}^{L}$$

$$\mathbf{J}_1^{e(o)} = diag\left(M_{c(s)l}^{(1)}(u_1,q_1)\right)_{l=0(1)}^{L}$$

$$\mathbf{H}_1^{e(o)} = diag\left(M_{c(s)l}^{(4)}(u_1,q_1)\right)_{l=0(1)}^{L}$$

$$\mathbf{H}_2^{e(o)} = diag\left(M_{c(s)l}^{(4)}(u_1,q_2)\right)_{l=0(1)}^{L}$$

$\mathbf{W}_e$ and $\mathbf{W}_o$ are the transformation matrices between the elliptical coordinate systems with different focal lengths [16], [23], [26]. In the case of confocal ellipses the matrices become unit matrices. For the non-confocal ellipses their elements take the following form:

$$[\mathbf{W}_e]_{ll'} = \frac{\int_0^{2\pi} dv\ ce_l(v,\bar{q}_1)ce_{l'}(v,q_1)}{\int_0^{2\pi} dv\ ce_l(v,q_1)ce_{l'}(v,q_1)}(i)^{l-l'}$$

$$[\mathbf{W}_o]_{ll'} = \frac{\int_0^{2\pi} dv\ se_l(v,\bar{q}_1)se_{l'}(v,q_1)}{\int_0^{2\pi} dv\ se_l(v,q_1)se_{l'}(v,q_1)}(i)^{l-l'}$$

The matrices $\mathbf{I}^{(\cdot)(\cdot)}$ and $\mathbf{I}_h^{(\cdot)(\cdot)}$ are composed of integrals of angular Mathieu functions, and their elements have the following form:

$$\begin{Bmatrix} (\mathbf{I}^{e_2e_\kappa})_{\iota l} \\ (\mathbf{I}^{e_2o'_\kappa})_{\iota l} \end{Bmatrix} = \int_0^{2\pi} dv\ ce_\iota(v,q_2) \begin{Bmatrix} ce_l(v,q_\kappa) \\ se'_l(v,q_\kappa) \end{Bmatrix}$$

$$\begin{Bmatrix} (\mathbf{I}^{o_2o_\kappa})_{\iota l} \\ (\mathbf{I}^{o_2e'_\kappa})_{\iota l} \end{Bmatrix} = \int_0^{2\pi} dv\ se_\iota(v,q_2) \begin{Bmatrix} se_l(v,q_\kappa) \\ ce'_l(v,q_\kappa) \end{Bmatrix}$$

$$\begin{Bmatrix} (\mathbf{I}_h^{e_2e_\kappa})_{\iota l} \\ (\mathbf{I}_h^{e_2o'_\kappa})_{\iota l} \end{Bmatrix} = \int_0^{2\pi} dv\ \frac{1}{h^{d_2,u_1}} ce_\iota(v,q_2) \begin{Bmatrix} ce_l(v,q_\kappa) \\ se'_l(v,q_\kappa) \end{Bmatrix}$$

$$\begin{Bmatrix} (\mathbf{I}_h^{o_2o_\kappa})_{\iota l} \\ (\mathbf{I}_h^{o_2e'_\kappa})_{\iota l} \end{Bmatrix} = \int_0^{2\pi} dv\ \frac{1}{h^{d_2,u_1}} se_\iota(v,q_2) \begin{Bmatrix} se_l(v,q_\kappa) \\ ce'_l(v,q_\kappa) \end{Bmatrix}$$

where $h^{d_2,u_1} = d_2\sqrt{\cosh^2(u_1)-\cos^2(v)}$ and $\iota,l = (0,\ldots,L)$ for even functions and $\iota,l=(1,\ldots,L)$ for odd functions. A prime symbol indicates derivatives of radial Mathieu functions with respect to the u variable or derivatives of angular Mathieu functions with respect to the v variable.

APPENDIX B
THE ELEMENTS OF MATRIX $\mathbf{Y}$

Matrix $\mathbf{Y}$, as defined in (21), has the following form:

$$\mathbf{Y}=\begin{bmatrix} \mathbf{Y}_{1e} & \mathbf{Y}_{1o} & \mathbf{Y}_{2e} & \mathbf{Y}_{2o} \\ \mathbf{Y}_{3e} & \mathbf{Y}_{3o} & \mathbf{0} & \mathbf{0} \end{bmatrix}$$

where its elements are horizontal vectors defined as follows:

$$\mathbf{Y}_{1e} = \left(\frac{\vartheta_2}{h^{d_2,u_1}} M_{cl}^{(4)}(u_1,q_2)ce'_l(v,q_2)\right)_{1,l=0}^{1,L}$$

$$\mathbf{Y}_{1o} = \left(\frac{\vartheta_2}{h^{d_2,u_1}} M_{sl}^{(4)}(u_1,q_2)se'_l(v,q_2)\right)_{1,l=1}^{1,L}$$

$$\mathbf{Y}_{2e} = \left(\frac{\beta_2}{h^{d_2,u_1}} M_{cl}^{'(4)}(u_1,q_2)ce_l(v,q_2)\right)_{1,l=0}^{1,L}$$

$$\mathbf{Y}_{2o} = \left(\frac{\beta_2}{h^{d_2,u_1}} M_{sl}^{'(4)}(u_1,q_2)se_l(v,q_2)\right)_{1,l=1}^{1,L}$$

$$\mathbf{Y}_{2e} = \left(M_{cl}^{(4)}(u_1,q_2)ce'_l(v,q_2)\right)_{1,l=0}^{1,L}$$

$$\mathbf{Y}_{2o} = \left(M_{sl}^{(4)}(u_1,q_2)se'_l(v,q_2)\right)_{1,l=1}^{1,L}$$

REFERENCES

[1] L. Josefsson and P. Persson, *Conformal Array Antenna Theory and Design*. Hoboken: John Wiley and Sons, Inc., 2006.

[2] P. Persson and R. G. Rojas, "Efficient technique for mutual coupling calculations between apertures on a PEC circular cylinder covered with a dielectric layer," *IEEE Antennas and Propag. Soc. Intern. Symp.*, vol. 3, pp. 252–255, Jul. 2001.

[3] Z. Sipus *et al.*, "An algorithm for calculating Green's functions of planar, circular cylindrical and spherical multilayer substrates," *App. Computational Electromag. Soc. Journal*, vol. 13, no. 3, pp. 243-254, 1998.

[4] A. F. Peterson and R. Mittra "Mutual admittance between slots in cylinders of arbitrary shape," *IEEE Trans. Antennas Propag.*, vol. 37, no. 7, pp. 858–864, Jul 1989.
[5] M. He and X. Xu, "Closed-form solutions for analysis of cylindrically conformal microstrip antennas with arbitrary radii," *IEEE Trans. Antennas Propag.*, vol. 53, no. 1, pp. 518–525, Jan. 2005.
[6] D. Khedrouchea *et al.* "Spectral-domain analysis of multilayer cylindricalrectangular microstrip antennas," *Engineering Analysis with Boundary Elements*, vol. 33, no. 7, pp. 930-939, Jul. 2009.
[7] S. M. Ali *et al.*, "Resonance in cylindrical-rectangular and wraparound microstrip structures," *IEEE Trans. Microw. Theory Techn.*, vol. 37, no. 11, pp. 1773–1783, Nov. 1989.
[8] K.-L. Wong *et al.*, "Resonance in a superstrate-loaded cylindrical-rectangular microstrip structure," *IEEE Trans. Microw. Theory Techn.*, vol. 41, no. 5, pp. 814–819, May 1993.
[9] T. M. Habashy *et al.*, "Input impedance and radiationpattern of cylindrical-rectangular and wraparound microstrip antennas," *IEEE Trans. Antennas Propag.*, vol. 38, no. 5, pp. 722–731, May 1990.
[10] R. Lech *et al.*, "An Analysis of Probe-fed Rectangular Patch Antennas with Multilayer and Multipatch Configurations on Cylindrical Surfaces," *IEEE Trans. Antennas Propag.*, vol. 62, no. 6, pp. 2935–2945, June 2014.
[11] T. Rylander and A. Bondeson, "Application of stable FEM-FDTD hybrid to scattering problems," *IEEE Trans. Antennas Propag.*, vol. 50, no. 2, pp. 141–144, Feb. 2002.
[12] He Mang and Xu Xiaowen, "Full-wave analysis and wide-band design of probe-fed multilayered cylindrical-rectangular microstrip antennas," *IEEE Trans. Antennas Propag.*, vol. 52, no. 7, pp. 1749–1757, Jul. 2004.
[13] V. B. Erturk *et al.*, "Analysis of finite arrays of axially directed printed dipoles on electrically large circular cylinders," *IEEE Trans. Antennas Propag.*, vol. 52, no. 10, pp. 2586–2595, Oct. 2004.
[14] B. Thors and L. Josefsson, "Radiation and scattering tradeoff design for conformal arrays," *IEEE Trans. Antennas Propag.*, vol. 51, no. 5, pp. 1069–1076, May 2003.
[15] P. Persson and L. Josefsson, "Calculating the mutual coupling between apertures on a convex circular cylinder using a hybrid UTD-MoM method," *IEEE Trans. Antennas Propag.*, vol. 49, no. 4, pp. 672–677, Apr. 2001.
[16] A. K. Hamid and M. I. Hussein, "Electromagnetic scattering by two parallel conducting elliptic cylinders: iterative solution," *IEEE International Symposium on Electromagnetic Compatibility, EMC '03*, vol. 1, pp. 21-24, 16 May 2003.
[17] A. Kusiek *et al.*, "Analysis of scattering from arbitrary configuration of elliptical obstacles using T-matrix representation," *IET Microw., Antennas Propag.*, vol. 2, no. 5, pp. 434-441, August 2008.
[18] N. J. Florous *et al.*, "Modeling of two-dimensional photonic crystal resonant cavities incorporating elliptically shaped dielectric cylinders," *IEEE Photonics Technology Letters*, vol. 17, no. 11, pp. 2316-2318, Nov. 2005.
[19] P. H. Pathak *et al.*, "A uniform GTD solution for the radiation from sources on a convex surface," *IEEE Trans. Antennas Propag.*, vol.29, no.4, pp.609,622, Jul 1981.
[20] P. H. Pathak, Nan Wang, "Ray analysis of mutual coupling between antennas on a convex surface," *IEEE Trans. Antennas Propag.*, vol. 29, no. 6, pp. 911-922, Nov. 1981.
[21] Chi-Wei Wu *et al.*, "Hybrid finite element-boundary integral method for cavities recessed in an elliptic cylinder," *IEEE Trans. Antennas Propag.*, vol. 51, no. 8, pp. 1829-1836, Aug. 2003.
[22] J. H. Richmond, "Axial slot antenna on dielectric-coated elliptic cylinder," *IEEE Trans. Antennas Propag.*, vol. 37, no. 10, pp. 1235-1241, Oct. 1989.
[23] A. Helaly and A. Sebak, "Radiation Conductance and Pattern of Array Antenna on a Non-Confocal Dielectric-Coated Elliptic Cylinder," *WSEAS Trans. on Communications*, iss. 11, vol. 7, pp. 1091-1101, Nov. 2008
[24] G. Amendola, "Analysis of the rectangular patch antenna printed on elliptic-cylindrical substrates," *IEE Proc. Microw., Antennas Propag.*, vol. 147, no. 3, pp. 187-194, Jun 2000.
[25] G. Angiulli *et al.*, "Radiation from dielectric coated elliptic conducting cylinder by assigned electric current distribution," *Prog. Electromagn. Res.*, vol. 57, 131-150, 2006.
[26] J. A. Stratton, *Electromagnetic Theory*, Mc-Graw Hill, New York, 1941.
[27] C. A. Balanis, *Antenna Theory: Analysis and Design*, Wiley, New York, 1997.
[28] W. C. Chew, *Waves and Fields in Inhomogeneous Media*, New York: Van Nostrand, 1990.
[29] C. Tokgoz and G. Dural, "Closed-form Green's functions for cylindrically stratified media," *IEEE Trans. Microw. Theory Techn.*, vol. 48, no. 1, pp. 40–49, Jan. 2000.
[30] P. Kowalczyk, "Complex Root Finding Algorithm Based on Delaunay Triangulation," *ACM Transactions on Mathematical Software* (in press).

Rafal Lech was born in Elblag, Poland, in 1977. He received the M.Sc.E.E. and Ph.D. (with honors) degrees from the Gdansk University of Technology, Gdansk, Poland, in 2001 and 2007, respectively. His main research interests are electromagnetic-wave scattering, numerical methods, filter design, complex materials, metamaterial applications at microwave frequencies, electromagnetic analysis of periodic structures, and antenna design.

Adam Kusiek was born in Mragowo, Poland, in 1980. He received the M.Sc.E.E. and Ph.D. (with honors) degrees from the Gdansk University of Technology, Gdansk, Poland, in 2004 and 2011, respectively. His research interests include developing of hybrid techniques to the analysis of complex structures, electromagnetic wave scattering, integrated nonreciprocal devices, antennas and passive structures for antenna feeding systems.

Wojciech Marynowski was born in Bydgoszcz, Poland, in 1980. He received the M.Sc.E.E. and Ph.D. (with honors) degrees from the Gdansk University of Technology, Gdansk, Poland, in 2004 and 2011, respectively. His research interests include electromagnetic wave propagation in complex materials, design of nonreciprocal planar microwave devices, wideband/ultra-wideband antennas and theirs feeding systems.